

Deep Patch Visual Odometry

Zachary Teed
Princeton University
zteed@princeton.edu

Lahav Lipson
Princeton University
llipson@princeton.edu

Jia Deng
Princeton University
jiadeng@princeton.edu

Abstract

We propose *Deep Patch Visual Odometry (DPVO)*, a new deep learning system for monocular Visual Odometry (VO). DPVO is accurate and robust while running at 2x-5x real-time speeds on a single RTX-3090 GPU using only 4GB of memory. We perform evaluation on standard benchmarks and outperform all prior work (classical or learned) in both accuracy and speed. Code is available at <https://github.com/princeton-vl/DPVO>.

1. Introduction

Visual Odometry (VO) is the task of estimating a robot’s position and orientation from visual measurements. In this work, we focus on most challenging case—monocular VO—where the only input is a monocular video stream. The goal of the system is to estimate the 6-DOF pose of the camera at every frame while simultaneously building a map of the environment.

VO is closely related to Simultaneous Localization and Mapping (SLAM). Like VO, SLAM systems aim to estimate camera pose and map the environment but also incorporate techniques for global corrections—such as loop closure and relocalization [3]. SLAM systems typically include a VO frontend which tracks incoming frames and performs local optimization. We observe that a significant portion of failures in SLAM systems occur in the frontend and hence focus on this aspect of the problem. However, we demonstrate that even without loop closure and global optimization, our approach is still accurate enough to outperform full SLAM systems.

Prior work typically treats VO as an optimization problem solving for a 3D model of the scene which best explains the visual measurements [3]. *Indirect* approaches first detect and match keypoints between frames, then solve for poses and 3D points which minimize the reprojection distance [4, 17, 22]. *Direct* approaches, on the other hand, operate directly on pixel intensities, attempting to solve for poses and depths which align the images [12, 13, 15]. The main issue with prior systems, both direct and indirect, is

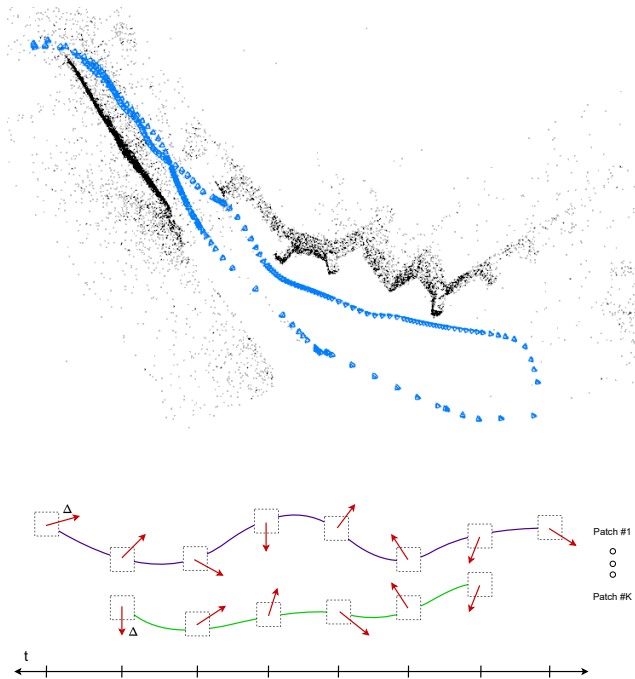


Figure 1. Deep Patch Visual Odometry (DPVO). Camera poses and a sparse 3D reconstruction (top) is obtained by iterative revisions of patch trajectories through time.

the lack of robustness. Failure cases are too frequent for many important applications such as autonomous vehicles. These failure cases typically stem from moving objects, lost feature tracks, and poor convergence.

Several deep learning approaches have been introduced to address the robustness issue. The main promise of deep learning is more reliable feature matching. DROID-SLAM [28] and VOLODOR [19, 20] use neural networks to estimate dense flow fields which are subsequently used to optimize depth and camera pose. Other approaches have used neural networks to match and verify a sparse set of keypoints [5, 10, 23, 25, 29]. Methods such as BANet [26] and DeepFactors [6] have used neural networks to parameterize the space of admissible depth maps. However, many of these systems come with a large computational cost

which make them impractical for real use cases. Furthermore, current deep VO systems are typically not as accurate as classical systems when evaluated on datasets on which they weren't trained [28].

We introduce DPVO, a novel patch-based deep VO system which overcomes these limitations. The central piece of our approach is a deep patch representation (Fig. 1). We use a neural network to extract a collection of patches from incoming frames. A recurrent neural network is then used to track each patch through time—alternating patch trajectory updates with a differentiable bundle adjustment layer. We train our entire system end-to-end on synthetic data but demonstrate strong generalization on real video.

Compared to prior deep-learning systems, the novelty of our approach lies in the tight integration of three key ingredients in a single architecture: (1) patch-based correspondence, (2) recurrent iterative updates, and (3) differentiable bundle adjustment. Patch-based correspondence improves efficiency and robustness over dense flow. Recurrent iterative updates and differentiable bundle adjustment allow end-to-end learning of reliable feature matching.

DPVO is accurate, efficient, and simple to implement. On a modern graphics card (RTX-3090), it runs 2x real-time using only 4GB of memory. We also provide a model which runs at 100fps on the EuRoC dataset [2] while still outperforming prior work. Runtime is constant for each frame and does not depend on the degree of camera motion. The implementation of the system is exceedingly simple with a minimal code base. New network architectures can be easily swapped in without any necessary change to the underlying VO implementation or logic. We hope that DPVO can serve as a test bed for future development of deep VO and SLAM systems.

2. Related Work

Visual Odometry (VO) systems aim to estimate robot state (position and orientation) from a video. Overtime, a VO system will accumulate drift, and modern SLAM methods incorporate techniques identify previously mapped landmarks to correct drift (i.e loop closure). VO can be considered a subproblem of SLAM with loop closures disabled [3].

Many different modalities of VO have been explored by past work, including visual-inertial odometry (VIO) [14,31] and stereo VO [13,32]. Here, we focus on the monocular case, where the only input is a monocular video stream. Early works approached the problem using filtering and maximum-likelihood methods [7,21]. Modern methods almost universally perform Maximum a Posteriori (MAP) estimation over factor graphs with Gaussian noise; in which case, the MAP estimate can be found by solving a non-linear least-squares optimization problem [9]. This problem has lead to the development of many libraries for optimizing

non-linear least-squares problems [1,8,16].

Among VO systems, our method borrows many core ideas of Direct Sparse Odometry (DSO) [12], a classical system based on least-squares optimization. Namely, we adopt a similar patch representation and reproject patches between frames to construct the objective function. Unlike DSO, the residuals are not based on intensity differences but instead predicted by a neural network which can pass information between patches and across patch lifetimes. Outlier rejection is automatically handled by the network, making our system comparable more robust than classical systems like DSO and ORB-SLAM [12,22]. One important component of classical systems is the careful selection of which image regions to use. We find, surprisingly, that our system works well on a small number (64 per frame) of *randomly* sampled image patches.

With regards to deep SLAM systems, our method is closely related to DROID-SLAM [28] but uses a different underlying representation. DROID-SLAM is an end-to-end deep SLAM system which showed good performance compared to both classical and deep baselines. Like our method, it works by iterating between motion updates and bundle adjustment. However, it estimates dense motion fields between selected pairs of frames which has a high computational cost and large memory footprint. While it is capable of real-time *on average*, its speed varies depending on the amount of motion in the video. Our method selects sparse patches from the video stream, with a constant runtime per frame and 5x faster inference than DROID-SLAM.

Prior works such as BA-Net [26] and Lindenberger et al. [18] have also embedded bundle adjustment layers in end-to-end differentiable network architectures. But BA-Net does not use patch-based correspondence. Lindenberger et al. [18] and Dusmanu et al. [11] have proposed neural networks which sit atop COLMAP [24] and perform subpixel-level refinement; these approaches are not however able to perform 3D reconstruction on their own and are subject to failure cases in the underlying SfM system.

3. Approach

Our network is trained and evaluated in an online setting. New frames are added one by one and optimization is performed in a local window of keyframes. Our approach has two main modules: the *patch extractor* (3.1) and the *update operator* (3.2). The *patch extractor* extracts a sparse collection of image patches from incoming frames. The *update operator* attempts to track these patches through time using a recurrent neural network alternating iterative updates with bundle adjustment.

Preliminaries: The scene is represented as a collection of N camera poses $\mathbf{T} \in \mathbb{SE}(3)^N$ and a set of M square image patches \mathbf{P} . Using \mathbf{d} to represent inverse depth and (\mathbf{x}, \mathbf{y})

pixel coordinates, we represent each patch as the $4 \times p^2$ homogeneous array

$$\mathbf{P}_i = \begin{pmatrix} \mathbf{x} \\ \mathbf{y} \\ \mathbf{1} \\ \mathbf{d} \end{pmatrix} \quad \mathbf{x}, \mathbf{y}, \mathbf{d} \in \mathbb{R}^{1 \times p^2} \quad (1)$$

where p is the width of the patch. We assume a constant depth for the full patch, meaning that it forms a fronto-parallel plan in the frame from which it was extracted. Letting j denote the index of the source frame from which patch \mathbf{P}_i was extracted we can reproject the patch onto another frame k

$$\mathbf{P}'_i \sim \mathbf{K} \mathbf{T}_k \mathbf{T}_j^{-1} \mathbf{K}^{-1} \mathbf{P}_i. \quad (2)$$

taking \mathbf{K} to be the 4×4 calibration matrix

$$\mathbf{K} = \begin{pmatrix} f_x & 0 & c_x & 0 \\ 0 & f_y & c_y & 0 \\ 0 & 0 & 1 & 0 \\ 0 & 0 & 0 & 1 \end{pmatrix} \quad (3)$$

The pixel coordinates $\mathbf{x}' = (x', y')$ can be recovered by dividing by the third element. For the rest of the paper, we use the shorthand $\mathbf{x}_{ij} = \omega_{ij}(\mathbf{T}, \mathbf{P})$ to denote the reprojection of patch i onto frame j in terms of pixel coordinates.

Patch Graph: We use a bipartite *patch graph* data structure to represent the patch lifetimes. Edges in the graph connect patches with frames. By default, the graph is constructed by adding an edge between each patch and every frame within distance r from the index of the frame it was extracted from. The reprojections of a patch onto all of its connected frames in the pose graph form the *trajectory* of the patch.

3.1. Feature and Patch Extraction

We use a pair of residual networks to extract features from the input images. One network extracts *matching* features while the other extracts *context* features. The first layer of each network is a 7×7 convolution with stride 2 followed by two residual blocks at 1/2 resolution (dimension 64) and 2 residual blocks at 1/4 resolution (dimension 128), such that the final feature map is one-quarter the input resolution. The architectures of the matching and context networks are identical with the exception that the matching network uses instance normalization and the context network uses no normalization. We construct a two-level feature pyramid by applying average pooling to the matching features with a 4×4 filter with stride 4.

We store the matching features for each frame. We additionally extract patches from both the matching and context feature maps. Patch centroids are randomly sampled then we use bilinear interpolation for feature retrieval. Unlike

DROID-SLAM, we never explicitly build correlation volumes. We instead store both frame and patch feature maps such that correlation features can be computed on-the-fly.

3.2. Update Operator

The purpose of the *update operator* is to update both poses and patches. This is done by performing revisions to patch trajectories as shown in Fig. 1. We provide a schematic overview of the operator in Fig. 2 and detail the individual components below. Each “+” operation in the diagram is a residual connection followed by layer normalization. The update operator acts on the patch graph, and each edge in the patch graph is augmented with a hidden state (dimension 384). When a new edge is added, the hidden state is initialized with zeros.

Correlation: For each edge (i, j) in the patch graph, we compute correlation features. We first use Eqn. 2 to reproject patch i in frame j : $\mathbf{x}_{ij} = \omega_{ij}(\mathbf{T}, \mathbf{P})$. Given patch features $\mathbf{g} \in \mathbb{R}^{p \times p \times D}$ and frame features $\mathbf{f} \in \mathbb{R}^{H \times W \times D}$, for each pixel (u, v) in patch i , we compute its correlation with a grid of pixels centered at the the reprojection of pixel (u, v) in frame j , using the inner product:

$$\mathbf{C}_{\mu\nu\lambda\rho} = \langle \mathbf{g}_{\mu\nu}, \mathbf{f}(\mathbf{x}_{ij} + \Delta_{\lambda\rho}) \rangle \quad (4)$$

where we take Δ to be a 7×7 integer grid centered at 0 indexed by λ and ρ , and $\mathbf{f}(\cdot)$ denotes bilinear sampling. We compute correlation features for both levels in the pyramid and concatenate the results. This operation is implemented as an optimized CUDA layer which leverages the regular grid structure of the interpolation step. This implementation is identical to the alternative correlation implementation used by RAFT [27] and is equivalent to indexing correlation volumes due to the linearity of the inner product and interpolation.

1D Temporal Convolution: We apply a 1D-Convolution in the temporal dimension to each patch trajectory. Since trajectories vary in length and keyframes are actively added and removed, it is not straightforward to implement convolution as a batched operation. Instead, for each edge (i, j) we index the features of its neighbors at $(i, j - 1)$ and $(i, j + 1)$, concatenate, then apply a linear projection. The temporal convolution allows the network to propagate information along each patch trajectory and model appearance changes of the patch through time.

SoftMax Aggregation: We use global message passing layers to propagate information between edges in the patch graph. This operation has appeared before in the context of graph neural networks. Given edge e and denoting its neighbors as $N(e)$ we define the channel-wise aggregation

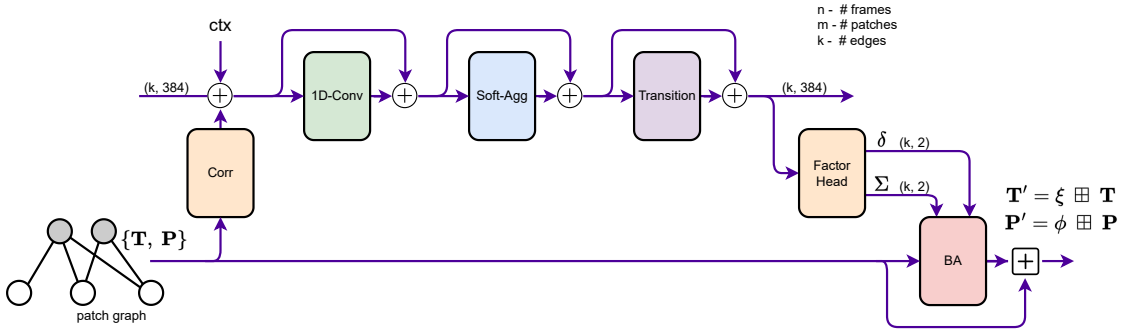


Figure 2. Schematic of the *update operator*. Correlation features are extracted from edges in the patch graph and injected into the hidden state alongside context features. We apply convolution, message passing and a transition block. The factor head produces trajectory revisions which are used by the bundle adjustment layer to update the camera poses and the depth of patches.

function

$$\psi \left(\left[\frac{\sum_{x \in N(e)} \sigma(x) \cdot \phi(x)}{\sum_{x \in N(e)} \sigma(x)} \right] \right) \quad (5)$$

where ψ and ϕ are linear layers and σ is a linear layer followed by a sigmoid activation. We perform two instantiations of soft aggregation: (1) patch aggregation where edges are neighbors if they connect to the same patch (2) frame aggregation where edges are neighbors if they connect to both the same source and destination frames.

Transition: The *transition* block in Fig. 2 is simply two residual units with Layer Normalization and ReLU nonlinearities.

Factor Head: The *factor head* consists of 2 MLPs with one hidden unit each. For each edge (i, j) in the pose graph, the first MLP predicts a trajectory update $\delta_{ij} \in \mathbb{R}^2$ —2d flow vector indicating how the reprojection of the patch center should be updated in 2D; the second MLP predicts a confidence weight map $\Sigma_{ij} \in \mathbb{R}^2$ which is bounded to $(0, 1)$ using a sigmoid activation.

Differentiable Bundle Adjustment: This layer in Fig. 2 operates globally on the patch graph and outputs updates to depth and camera poses. The predicted factors (δ, Σ) are used to define an optimization objective:

$$\sum_{(i,j) \in \mathcal{E}} \|\hat{\omega}_{ij}(\mathbf{T}, \mathbf{P}) - [\hat{\mathbf{x}}_{ij} + \delta_{ij}]\|_{\Sigma_{ij}}^2 \quad (6)$$

where $\|\cdot\|_{\Sigma}$ is the Mahalanobis distance and $\hat{\mathbf{x}}_{ij}$ denotes the center of patch \mathbf{x}_{ij} . We apply two Gauss-Newton iterations to the linearized objective, optimizing the camera poses as well as the inverse depth component of the patch while keeping the pixel coordinates constant. This optimization seeks to refine the camera poses and depth such that the induced trajectory updates agree with the predicted

trajectory updates. Similar to DROID-SLAM [28], we apply the Schur complement trick for efficient decomposition, and backpropagate gradients through the Gauss-Newton iterations.

3.3. Training and Supervision

DPVO is implemented using PyTorch. We train our network on the TartanAir dataset. On each training sequence, we precompute optical flow magnitude between all pairs of frames using the ground truth poses and depth. During training, we sample trajectories where frame-to-frame optical flow magnitude is between 16px and 72px. This ensures that training instances are generally difficult but not impossible.

We apply supervision to poses and induced optical flow (i.e. trajectory updates), supervising each intermediate output of the update operator and detach the poses and patches from the gradient tape prior to each update.

Pose Supervision: We scale the predicted trajectory to match the groundtruth using the Umeyama alignment algorithm [30]. Then for every pair of poses (i, j) , we supervise on the error

$$\sum_{(i,j) \ i \neq j} \|\text{Log}[(\mathbf{G}_i^{-1} \mathbf{G}_j)^{-1} (\mathbf{T}_i^{-1} \mathbf{T}_j)]\| \quad (7)$$

where \mathbf{G} is the ground truth and \mathbf{T} are the predicted poses.

Flow Supervision: We additionally supervise on the distance between the induced optical flow and the ground truth optical flow between each patch and frames within two timestamps from the frame which each patch was extracted. Each patch induces a $p \times p$ flow field. We take the minimum of all $p \times p$ errors.

The final loss is the weighted combination

$$\mathcal{L} = 10\mathcal{L}_{pose} + 0.1\mathcal{L}_{flow}. \quad (8)$$

Training Details: We train for a total of 240k iterations on a single RTX-3090 GPU with a batch size of 1. Training takes

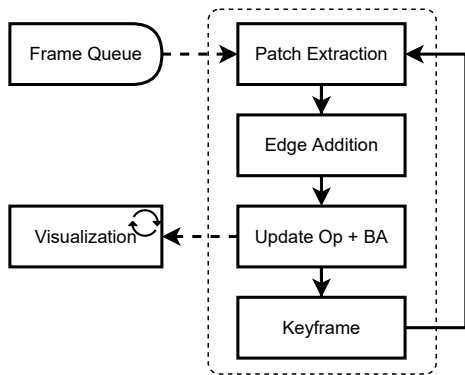


Figure 3. Overview of the VO System.

3.5 days. We use the AdamW optimizer and start with an initial learning rate of $8e-5$ which is decayed linearly during training. We apply standard augmentation techniques such as resizing and color jitter.

We train on sequences of length 15. The first 8 frames are used for initialization while the next 7 frames are added one at a time. We unroll 18 iterations of the update operator during training. For the first 1k training steps, we fix poses with the ground truth and only ask the network to estimate the depth of the patches. Afterwards, the network is required to estimate both poses and depth.

4. VO System

In this section, we cover several key implementation details necessary for turning our network into a complete visual odometry system. The logic of the system is primarily implemented in Python with bottleneck operations such as bundle adjustment and visualization implemented in c++ and CUDA. Compared to other VO system, DPVO is exceedingly simple and requires minimal design choices.

Initialization: We use 8 frames for initialization. We add new patches and frames until 8 frames are accumulated then run 12 iterations of our update operator. There needs to be some camera motion for initialization; hence, we only accumulate frames with an average flow magnitude of at least 8 pixels from the prior frame.

Expansion: When a new frame is added we extract features and patches. The pose of the new frame is initialized using a constant velocity motion model. The depth of the patch is initialized as the median depth of all the patches extracted from the previous 3 frames.

We connect each patch to every frame within distance r from the frame index the patch was extracted. This means that when a new patch is added, we add edges between that patch and the previous r keyframes. When a new frame is added, we add edges between each patch extracted in the last r keyframes with the new frame. This strategy means

that the patch graph will always has a maximum size ensuring worst case constant runtime.

Optimization: Following the addition of edges we run one iteration of the update operator followed by two bundle adjustment iterations. We fix the poses of all but the last 10 keyframes. The inverse depths of all patches are free parameters. The patches are removed from optimization once they fall outside the optimization window.

Keyframing: The most recent 3 frames are always taken to be keyframes. After each update, we compute the optical flow magnitude between keyframe $t - 5$ and $t - 3$. If this is less than 64px, we remove the keyframe at $t - 4$. When a keyframe is removed, we store the relative pose between its neighbors such that the full pose trajectory can be recovered for evaluation.

Visualization: Reconstructions are visualized interactively using a separate visualization thread. Our visualizer is implemented using the Pangolin library¹. It directly reads from PyTorch tensors avoiding all unnecessary memory copies from CPU to GPU. This means that the visualizer has very little overhead—only slowing the full system down by approximately 10%.

5. Experiments

We evaluate DPVO on the TartanAir [34] and EuRoC [2] benchmarks. On each dataset, we give a measure of the variance by running multiple trials each with a different set of patches and report the median, worst and best results obtained. Example reconstructions on the TartanAir and ETH3D datasets are shown in Fig. 4.

5.1. Tartan Air [34]

Validation Split: We use the same 32-sequence validation split as DROID-SLAM and report aggregated results in Fig. 5 and compare with DROID-SLAM and ORB-SLAM3. We run our method 3 times on each sequence and aggregate the results. In the $[0, 1]m$ error window, we get an AUC of 0.80 compared to 0.71 for DROID-SLAM.

Test Split: We also report results on the test-split used in the ECCV 2020 SLAM competition compared to state-of-the-art methods. Classical methods such as DSO and ORB-SLAM fail on more than 80% of the sequences, hence we use COLMAP as a classical baseline as it was used in the two winning solution of the ECCV SLAM competition. For our method, we run five times on each sequence and report the best, median and worst results.

We benchmark two versions of DROID-SLAM: the full version and a version where loop closure and global bundle adjustment is disabled (DROID-VO). DROID-VO is more

¹<https://github.com/stevenlovegrove/Pangolin>

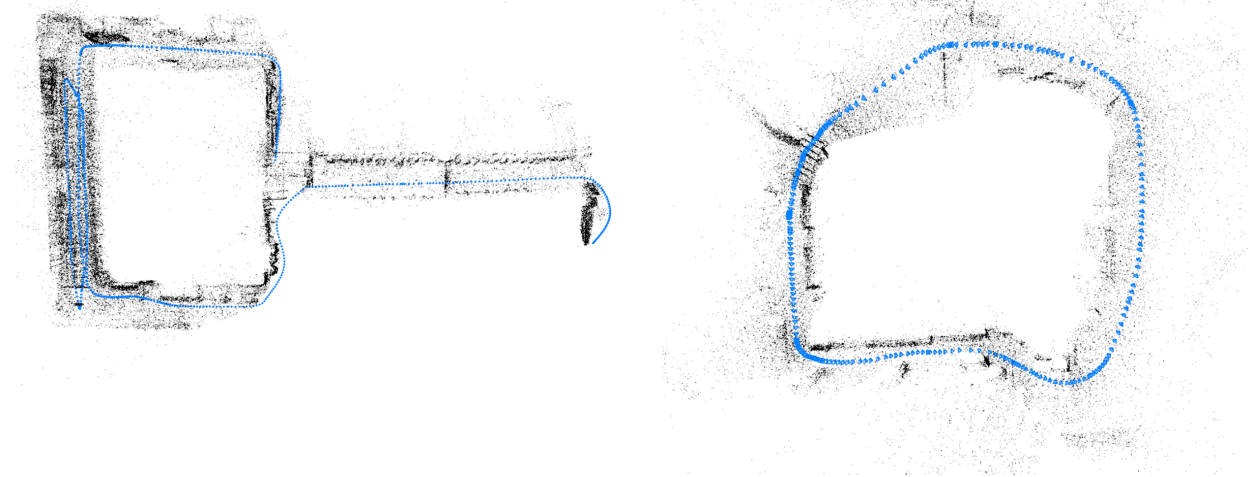


Figure 4. Example reconstructions: TartanAir (left) and ETH3D (right)

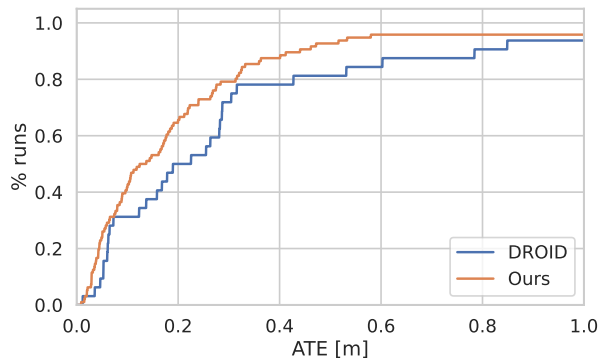


Figure 5. Results on the TartanAir [34] validation split. Our method gets an AUC of 0.80 compared to 0.71 for DROID-SLAM while running 4x faster.

comparable to our method as we only perform local optimization. We outperform both methods with an error 40% lower than DROID-SLAM and 64% lower than DROID-VO. COLMAP takes 2 days complete the 16 sequences and typically produces broken reconstructions which lead to large errors in evaluation.

5.2. EuRoC MAV [2]

In Tab. 2 we benchmark on the EuRoC [2] dataset and compare to other visual odometry methods including SVO [15], DSO [12] and the visual odometry version of DROID-SLAM [27]. Video from the EuRoC benchmark is recorded at 20fps. Like DROID-SLAM, we skip every other frame, doubling the effective frame rate of the system. We benchmark two configuration settings: Ours-60fps uses 96 patches per image and a 10 frame optimization window and Ours-100fps which uses 48 patches and a 7 frame

	ORB-SLAM3 [4]	DSO [12]	COLMAP [24]	DROID [28]	DROID-VO	Ours
ME000	13.61	9.65	15.20	0.17	0.22	0.16
ME001	16.86	3.84	5.58	0.06	0.15	0.11
ME002	20.57	12.20	10.86	0.36	0.24	0.11
ME003	16.00	8.17	3.93	0.87	1.27	0.66
ME004	22.27	9.27	2.62	1.14	1.04	0.31
ME005	9.28	2.94	14.78	0.13	0.14	0.14
ME006	21.61	8.15	7.00	1.13	1.32	0.30
ME007	7.74	5.43	18.47	0.06	0.77	0.13
MH000	15.44	9.92	12.26	0.08	0.32	0.21
MH001	2.92	0.35	13.45	0.05	0.13	0.04
MH002	13.51	7.96	13.45	0.04	0.08	0.04
MH003	8.18	3.46	20.95	0.02	0.09	0.08
MH004	2.59	-	24.97	0.01	1.52	0.58
MH005	21.91	12.58	16.79	0.68	0.69	0.17
MH006	11.70	8.42	7.01	0.30	0.39	0.11
MH007	25.88	7.50	7.97	0.07	0.97	0.15
Average	14.38	7.32	12.50	0.33	0.58	0.21

Table 1. Results on the TartanAir monocular test split. Results are reported as ATE with scale alignment. For our method, we report the median of 5 runs (full results logs are provided on our github)

optimization window. These runtimes are strictly enforced; 60fps / 100fps is the *slowest* frame rates the system will ever achieve. Following prior work, we run our system five times on each sequence, randomly sampling a different collection of patches, and report the median result. Full result logs are provided with our code. Our 3x real-time system outperforms prior work on the majority of the EuRoC sequences. The average error is 43% lower than DROID-VO [28]. Even the 100fps system outperforms DROID-VO on most video.

	MH01	MH02	MH03	MH04	MH05	V101	V102	V103	V201	V202	V203	Avg
TartanVO [33]	0.639	0.325	0.550	1.153	1.021	0.447	0.389	0.622	0.433	0.749	1.152	0.680
SVO [15]	0.100	0.120	0.410	0.430	0.300	0.070	0.210	X	0.110	0.110	1.080	-
DSO [12]	0.046	0.046	0.172	3.810	0.110	0.089	0.107	0.903	0.044	0.132	1.152	0.601
DROID-VO [28]	0.163	0.121	0.242	0.399	0.270	0.103	0.165	0.158	0.102	0.115	0.204	0.186
Ours-60fps	0.087	0.055	0.158	0.137	0.114	0.050	0.140	0.086	0.057	0.049	0.211	0.105
Ours-100fps	0.101	0.067	0.177	0.181	0.123	0.053	0.158	0.095	0.095	0.063	0.310	0.129

Table 2. Monocular SLAM on the EuRoC datasets, ATE[m] compared to other visual odometry methods.

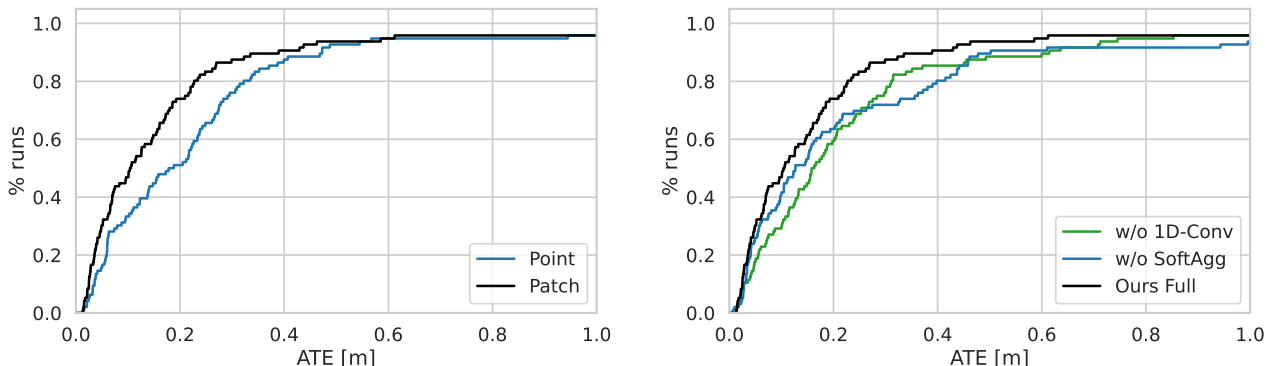


Figure 6. Ablation experiments. (Left) We show the importance of using patches over point features. (Right) Removal of different components of the update operator degrades accuracy.

5.3. Ablations

We perform ablation experiments on the TartanAir validation split and show results in Fig. 6. We use the same parameter settings in all experiments with augmentation disabled. We run each ablation experiment three times on the validation split and aggregate the results.

Point vs Patch Features: In Fig. 6 (left), we demonstrate the importance of the patch over simply using point features (i.e. 1x1 patches). The patch features encode local context which is lacking with point features. The additional information stored in the correlation features allows for more precise tracking.

Update Operator: In Fig. 6 (right), we test the effect of removing various components from the update operator. Both removing 1D-Convolution and Softmax-Aggregation degrade performance on the validation set.

Timing: The default configuration of our system runs at 40fps. We plot the distribution of runtimes over multiple frames and runs in Fig. 7. The design of our system leads to very little variance in latency.

6. Conclusion

DPVO is a new deep visual odometry system built using a sparse patch representation. It is accurate and efficient, capable of running at 2x-5x real-time frame rates with min-

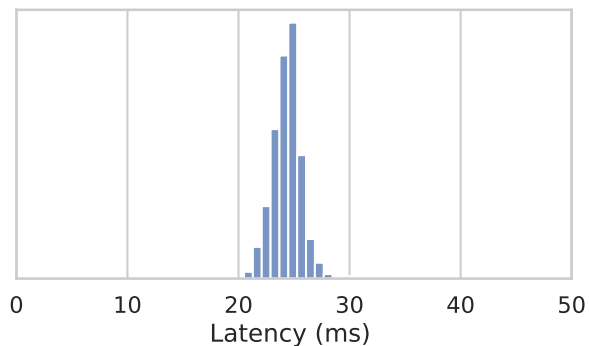


Figure 7. Runtime distribution. Our system averages 40fps with each new frame taking 25ms to process. The distribution is very centralized and never drops below 30fps.

imal memory requirements.

Acknowledgments: This work was partially supported by the Qualcomm Innovation Fellowship, the Princeton University Jacobus Fellowship, and National Science Foundation Award IIS-1942981.

References

- [1] Sameer Agarwal, Keir Mierle, and The Ceres Solver Team. Ceres Solver, 3 2022. 2

- [2] Michael Burri, Janosch Nikolic, Pascal Gohl, Thomas Schneider, Joern Rehder, Sammy Omari, Markus W Achtelik, and Roland Siegwart. The euroc micro aerial vehicle datasets. *The International Journal of Robotics Research*, 35(10):1157–1163, 2016. [2](#), [5](#), [6](#)
- [3] Cesar Cadena, Luca Carlone, Henry Carrillo, Yasir Latif, Davide Scaramuzza, José Neira, Ian Reid, and John J Leonard. Past, present, and future of simultaneous localization and mapping: Toward the robust-perception age. *IEEE Transactions on robotics*, 32(6):1309–1332, 2016. [1](#), [2](#)
- [4] Carlos Campos, Richard Elvira, Juan J Gómez Rodríguez, José MM Montiel, and Juan D Tardós. Orb-slam3: An accurate open-source library for visual, visual-inertial, and multi-map slam. *IEEE Transactions on Robotics*, 37(6):1874–1890, 2021. [1](#), [6](#)
- [5] Christopher B Choy, JunYoung Gwak, Silvio Savarese, and Manmohan Chandraker. Universal correspondence network. *Advances in neural information processing systems*, 29, 2016. [1](#)
- [6] Jan Czarnowski, Tristan Laidlow, Ronald Clark, and Andrew J Davison. Deepfactors: Real-time probabilistic dense monocular slam. *IEEE Robotics and Automation Letters*, 5(2):721–728, 2020. [1](#)
- [7] Andrew J Davison. Real-time simultaneous localisation and mapping with a single camera. In *Computer Vision, IEEE International Conference on*, volume 3, pages 1403–1403. IEEE Computer Society, 2003. [2](#)
- [8] Frank Dellaert. Factor graphs and gtsam: A hands-on introduction. Technical report, Georgia Institute of Technology, 2012. [2](#)
- [9] Frank Dellaert, Michael Kaess, et al. Factor graphs for robot perception. *Foundations and Trends® in Robotics*, 6(1-2):1–139, 2017. [2](#)
- [10] Daniel DeTone, Tomasz Malisiewicz, and Andrew Rabinovich. Superpoint: Self-supervised interest point detection and description. In *Proceedings of the IEEE conference on computer vision and pattern recognition workshops*, pages 224–236, 2018. [1](#)
- [11] Mihai Dusmanu, Johannes L Schönberger, and Marc Pollefeys. Multi-view optimization of local feature geometry. In *European Conference on Computer Vision*, pages 670–686. Springer, 2020. [2](#)
- [12] Jakob Engel, Vladlen Koltun, and Daniel Cremers. Direct sparse odometry. *IEEE transactions on pattern analysis and machine intelligence*, 40(3):611–625, 2017. [1](#), [2](#), [6](#), [7](#)
- [13] Jakob Engel, Thomas Schöps, and Daniel Cremers. Lsd-slam: Large-scale direct monocular slam. In *European conference on computer vision*, pages 834–849. Springer, 2014. [1](#), [2](#)
- [14] Christian Forster, Luca Carlone, Frank Dellaert, and Davide Scaramuzza. Imu preintegration on manifold for efficient visual-inertial maximum-a-posteriori estimation. Georgia Institute of Technology, 2015. [2](#)
- [15] Christian Forster, Matia Pizzoli, and Davide Scaramuzza. Svo: Fast semi-direct monocular visual odometry. In *2014 IEEE international conference on robotics and automation (ICRA)*, pages 15–22. IEEE, 2014. [1](#), [6](#), [7](#)
- [16] Giorgio Grisetti, Rainer Kümmerle, Hauke Strasdat, and Kurt Konolige. g2o: A general framework for (hyper) graph optimization. In *Proceedings of the IEEE international conference on robotics and automation (ICRA)*, Shanghai, China, pages 9–13, 2011. [2](#)
- [17] Stefan Leutenegger, Paul Furgale, Vincent Rabaud, Margarita Chli, Kurt Konolige, and Roland Siegwart. Keyframe-based visual-inertial slam using nonlinear optimization. *Proceedings of Robotics Science and Systems (RSS) 2013*, 2013. [1](#)
- [18] Philipp Lindenberger, Paul-Edouard Sarlin, Viktor Larsson, and Marc Pollefeys. Pixel-perfect structure-from-motion with featuremetric refinement. In *Proceedings of the IEEE/CVF International Conference on Computer Vision*, pages 5987–5997, 2021. [2](#)
- [19] Zhixiang Min and Enrique Dunn. Voldor+ slam: For the times when feature-based or direct methods are not good enough. In *2021 IEEE International Conference on Robotics and Automation (ICRA)*, pages 13813–13819. IEEE, 2021. [1](#)
- [20] Zhixiang Min, Yiding Yang, and Enrique Dunn. Voldor: Visual odometry from log-logistic dense optical flow residuals. In *Proceedings of the IEEE/CVF Conference on Computer Vision and Pattern Recognition*, pages 4898–4909, 2020. [1](#)
- [21] Anastasios I Mourikis, Stergios I Roumeliotis, et al. A multi-state constraint kalman filter for vision-aided inertial navigation. In *ICRA*, volume 2, page 6, 2007. [2](#)
- [22] Raul Mur-Artal, Jose Maria Martinez Montiel, and Juan D Tardos. Orb-slam: a versatile and accurate monocular slam system. *IEEE transactions on robotics*, 31(5):1147–1163, 2015. [1](#), [2](#)
- [23] Paul-Edouard Sarlin, Daniel DeTone, Tomasz Malisiewicz, and Andrew Rabinovich. Superglue: Learning feature matching with graph neural networks. In *Proceedings of the IEEE/CVF conference on computer vision and pattern recognition*, pages 4938–4947, 2020. [1](#)
- [24] Johannes L Schonberger and Jan-Michael Frahm. Structure-from-motion revisited. In *Proceedings of the IEEE conference on computer vision and pattern recognition*, pages 4104–4113, 2016. [2](#), [6](#)
- [25] Jiaming Sun, Zehong Shen, Yuang Wang, Hujun Bao, and Xiaowei Zhou. Loftr: Detector-free local feature matching with transformers. In *Proceedings of the IEEE/CVF conference on computer vision and pattern recognition*, pages 8922–8931, 2021. [1](#)
- [26] Chengzhou Tang and Ping Tan. Ba-net: Dense bundle adjustment network. *arXiv preprint arXiv:1806.04807*, 2018. [1](#), [2](#)
- [27] Zachary Teed and Jia Deng. Raft: Recurrent all-pairs field transforms for optical flow. In *European conference on computer vision*, pages 402–419. Springer, 2020. [3](#), [6](#)
- [28] Zachary Teed and Jia Deng. Droid-slam: Deep visual slam for monocular, stereo, and rgb-d cameras. *Advances in Neural Information Processing Systems*, 34:16558–16569, 2021. [1](#), [2](#), [4](#), [6](#), [7](#)
- [29] Prune Truong, Martin Danelljan, Luc Van Gool, and Radu Timofte. Learning accurate dense correspondences and when to trust them. In *Proceedings of the IEEE/CVF Conference*

- on *Computer Vision and Pattern Recognition*, pages 5714–5724, 2021. 1
- [30] Shinji Umeyama. Least-squares estimation of transformation parameters between two point patterns. *IEEE Transactions on Pattern Analysis & Machine Intelligence*, 13(04):376–380, 1991. 4
- [31] Lukas Von Stumberg, Vladyslav Usenko, and Daniel Cremers. Direct sparse visual-inertial odometry using dynamic marginalization. In *2018 IEEE International Conference on Robotics and Automation (ICRA)*, pages 2510–2517. IEEE, 2018. 2
- [32] Rui Wang, Martin Schworer, and Daniel Cremers. Stereo dso: Large-scale direct sparse visual odometry with stereo cameras. In *Proceedings of the IEEE International Conference on Computer Vision*, pages 3903–3911, 2017. 2
- [33] Wenshan Wang, Yaoyu Hu, and Sebastian Scherer. Tartanvo: A generalizable learning-based vo. *arXiv preprint arXiv:2011.00359*, 2020. 7
- [34] Wenshan Wang, DeLong Zhu, Xiangwei Wang, Yaoyu Hu, Yuheng Qiu, Chen Wang, Yafei Hu, Ashish Kapoor, and Sebastian Scherer. Tartanair: A dataset to push the limits of visual slam. In *2020 IEEE/RSJ International Conference on Intelligent Robots and Systems (IROS)*, pages 4909–4916. IEEE, 2020. 5, 6